Analyst

PAPER

View Article Online
View Journal | View Issue

Cite this: *Analyst*, 2016, **141**, 2733

Au nanoparticle decorated graphene nanosheets for electrochemical immunosensing of p53 antibodies for cancer prognosis†

Reda Elshafey,[a,b] Mohamed Siaj*[b] and Ana C. Tavares*[a]

Received 6th January 2016,
Accepted 2nd February 2016

DOI: 10.1039/c6an00044d

www.rsc.org/analyst

The accurate quantification of the level of p53 antibodies in serum is crucial for cancer prognosis. We report a novel and sensitive label-free immunosensor based on gold nanoparticles (Au NPs) self-assembled onto electrochemically reduced graphene oxide (ERGO) for the detection of p53 antibodies. An electrografted *p*-aminophenol organic layer was used to immobilize graphene oxide (GO) onto the surface of screen printed carbon electrodes (SPCE). The Au NP/ERGO hybrid interface provides a large surface area for the effective immobilization of p53 antigens, as well as it ascertains the bioactivity and stability of immobilized p53 antigens. Scanning electron microscope, Raman and X-ray photoelectron spectroscopies were used to monitor the sensor fabrication and cyclic voltammetry was used to quantify the extent of Au NPs' surface coverage by p53 antigens. Square wave voltammetry (SWV) of a $[Fe(CN)_6]^{3-/4-}$ couple was employed to investigate the immunosensor fabrication and to monitor the binding events between p53 antigens and p53 antibodies. Under optimized experimental conditions, the biosensor displayed good sensitivity and specificity. The p53 antibodies were detected in a concentration as low as 0.088 pg mL^{-1} with a linear range from 0.1 pg mL^{-1} to 10 ng mL^{-1}. The high sensitivity of the immunosensor may derive from the high loading of p53 antibodies on Au NPs which increases the number of binding events.

Introduction

Cancer is the most commonly occurring disease worldwide and the second leading cause of death following heart disease.[1] The integration of serum auto-antibodies with other conventional markers[2,3] has potential for cancer screening and prognosis.[4,5] p53, a tumor suppressor protein, "the guardian of the genome", plays a crucial role in the regulation of the cell cycle, DNA repair, and programmed cell death.[5,6] Mutations of the p53 gene are the most common genetic alterations in human cancers.[7,8] These mutations lead to the accumulation of the mutated p53 protein which acts as an antigen with subsequent production of antibodies against it. p53 antibodies have been observed in the serum of patients with different cancers such as breast,[9] liver,[10] ovarian[11] and lung.[12] Because of the high clinical significance of the serum p53 antibody, it may serve as a potential indicator for malignancy screening and prognosis.[11,13] Generally, the conventional detection routes for p53 antibodies are western blot,[14] enzyme-linked immunosorbent assay (ELISA),[15] and optical electrochemiluminescence based assays.[16] Biosensors are being developed as alternatives to these traditional approaches for point-of-care applications.[17–20] However for p53 antibodies, only two biosensors have been developed.[21,22] One is a peptide-based impedimetric biosensor in which peptides were immobilized on functionalized gold microelectrodes. In addition, the epitopes responsible for the selective detection of p-53 antibodies were identified. The other sensor is based on a microcantilever modified by the p53 antigen and the deflection is measured using integrated piezoresistors. The detection range of this sensor is 20 ng mL^{-1} to 20 μg mL^{-1}.

Graphene-based/Au nanocomposites have been used in various applications including electrochemical biosensing of cancer markers.[23–26] These nanocomposites combine the intrinsic properties of Au nanoparticles (NPs) with those of graphene-based materials, such as high electrical conductivity and enhanced surface area, which are essential for the high sensitivity of biosensors. Owing to their intrinsic properties, reduced graphene oxide and gold nanoparticles could form an ideal platform for the p53 protein immobilization and sensitive assay of p53 antibodies.

Various approaches have been used for the preparation of graphene-based/Au NP modified surfaces. These include, the

[a]*Institut National de la Recherche Scientifique – Énergie, Matériaux et Télécommunications, Varennes, Québec, Canada J3X 1S2. E-mail: ana.tavares@emt.inrs.ca; Tel: +1 514 228 6947*
[b]*Département de Chimie et Biochimie, NanoQAM, CQMF, Université du Québec à Montréal, Montréal, Québec, Canada H3C 3P8. E-mail: siaj.mohamed@uqam.ca; Tel: +1 514 987 3000 # 1921*

†Electronic supplementary information (ESI) available. See DOI: 10.1039/c6an00044d

simultaneous formation of reduced graphene oxide and Au NPs by electrodeposition,[27] layer-by-layer assembly of reduced graphene oxide and Au NPs,[28,29] electrodeposition of Au NPs onto the graphene modified surfaces,[30] dropcasting of graphene followed by electrodeposition of Au NPs,[31] and dropcasting of graphene oxide/Au NP suspensions.[32]

Thus, in this study we propose a novel platform for the sensitive and selective detection of the p53 antibody. Au NPs are self-assembled onto a thiolated electrochemically reduced graphene oxide (ERGO) film assembled onto the surface of a screen printed carbon electrode (SPCE) through a *p*-aminophenyl linker. The self-assembly method has been proposed for preparation of graphene modified surfaces to overcome the drawbacks of other methods such as uncontrolled thickness and inhomogeneity of the layer. Some reports have discussed the usage of other linkers either physically adsorbed such as a diamine linker onto the indium tin oxide surface,[33] or electrografted such as 3-aminopropyltriethoxysilane on an activated glassy carbon electrode[34] and aminoethyl benzenediazonium onto the indium tin oxide surface.[35] The terminal carboxylic groups of the ERGO were then activated through carbodiimide chemistry for ERGO thiolation with cysteamine. Subsequently, the thiolated ERGO was used to assemble Au NPs *via* Au–S bonds (ERGO/cys/Au NPs). The p53 protein was immobilized onto the Au NPs through the interactions of the positively charged p53 amine groups and the NPs (ERGO/cys/AuNP/p53). The sensor modification was monitored by surface characterization and electrochemical techniques such as scanning electron microscopy (SEM), Raman spectroscopy, X-ray photoelectron spectroscopy (XPS), cyclic voltammetry and square wave voltammetry (SWV). The drop in the SWV peak current of $[Fe(CN)_6]^{3-/4-}$ was attributed to the response of the p53 antibody binding to the sensor. This biosensor has the potential to be used as a tool for early cancer diagnosis, by integrating it with other conventional tests.

Experimental section

Materials

Natural graphite flakes (+100 mesh, ≥75%), potassium permanganate (99%), sulphuric acid (98%), phosphoric acid (85%), hydrogen peroxide (30%), anhydrous ethanol and anhydrous ether with ACS grade or higher were used, 4-nitroaniline, potassium ferrocyanide $K_4Fe(CN)_6$, potassium ferricyanide $K_3Fe(CN)_6$, disodium hydrogen orthophosphate, potassium dihydrogen orthophosphate potassium chloride, sodium nitrite, hydrochloric acid, bovine serum albumin (BSA), 1-ethyl-3-(3-dimethylaminopropyl) carbodiimide hydrochloride (EDC), *N*-hydroxysuccinimide (NHS), 2-(*N*-morpholino) ethanesulfonic acid (MES), cysteamine hydrochloride, hydrogen tetrachloroaurate(III)hydrate ($HAuCl_4{\cdot}3H_2O$), sodium citrate, mouse monoclonal antibodies to EGFR, PDGFRα and bovine serum albumin (BSA), were obtained from Sigma-Aldrich (Ontario, Canada). The p53 protein and its mouse monoclonal anti-p53 antibody were purchased from Abcam (Cambridge, USA). Tween 20, potassium chloride, sodium hydroxide, potassium hydroxide, sodium chloride, and hydrochloric acid were purchased from Bioshop (Ontario, Canada) and used as received. Screen printed carbon electrodes (SPCEs) (2.64 mm^2) were obtained from BioDevice Technology Ltd (Japan).

Fabrication of SPCE/ERGO/Au NP platform

Scheme 1 summarizes the fabrication steps of the biosensor. Graphene oxide (GO) was prepared by using the modified Hummers method.[36] GO assembled SPCE surfaces were obtained as follows: the SPCEs were grafted with a *p*-nitrophenyl film by electrochemical reduction of the *in situ* generated *p*-nitrophenyl diazonium salt in acidic aqueous solution (Fig. S1A, ESI†). The electrochemical reduction of the nitro groups to the amine groups has been performed as previously reported.[37] The produced *p*-aminophenyl modified SPCE

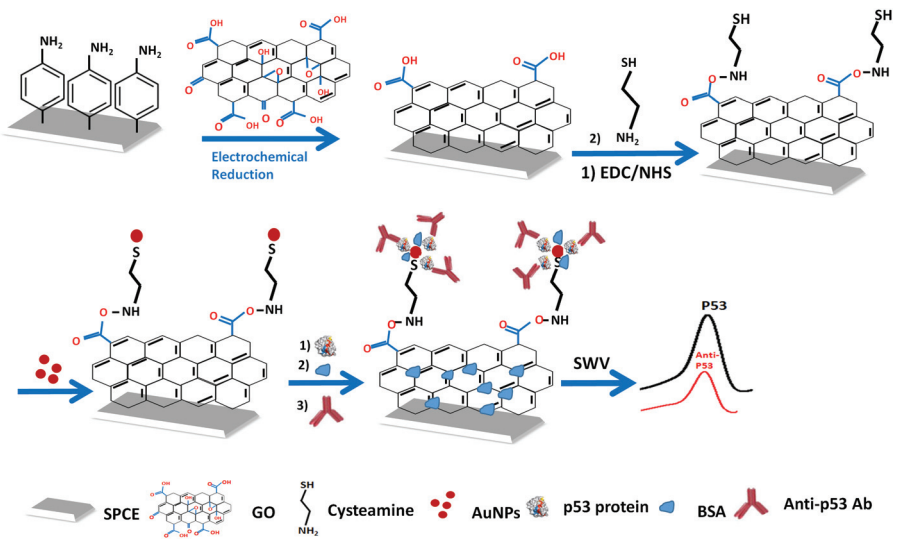

Scheme 1 Schematic illustration for fabrication of the p53-Ab immunosensor.

electrodes were then immersed in a GO aqueous solution (0.05 mg mL^{-1}) for 2 h to obtain the SPCE/GO electrode. SPCE/ERGO electrodes were obtained by applying a potential of −1.2 V (*vs.* Ag/AgCl) for 900 s to the GO-modified SPCE in a PBS pH 7.4 solution. The electrochemical characterization of the assembled GO and ERGO on the SPCE surface is presented in detail in the ESI (Fig. S1C and D†). The ERGO/SPCEs were further modified with thiol (–SH) groups by binding the COOH groups of ERGO to the amine (NH_2) groups of cysteamine through amide bonds. The SH modified ERGO/SPCEs were used thereafter for self-assembly of Au NPs (ERGO/cys/Au NPs).

Colloidal gold nanoparticles (Au NPs) were prepared using a published protocol.[38] Briefly, a 100 mL solution of 0.01% tetrachloroauric acid $HAuCl_4$ was boiled under vigorous stirring, and 5 mL of 1% trisodium citrate solution was rapidly added to the boiling gold chloride solution. After 10 min, the solution turned deep red, indicating the formation of colloidal Au NPs. The suspension was left under stirring while cooling down to room temperature. The UV–vis spectrum of Au NPs is shown in Fig. S2 (ESI†) in which the characteristic peak at 518 nm confirms the formation of Au NPs.

Immunosensor assembly

The p53 antibody immunosensors (p53/Au NP/ERGO/SPCE) were assembled by immobilizing the p53 protein (50 μg mL^{-1} in 0.1 M PBS, pH 8.5) onto the Au NP modified electrodes through electrostatic interactions between the p53 amine groups and the Au NPs overnight at 4 °C. Following p53 incubation, the electrodes were thoroughly rinsed in 0.1% Tween-PBS (pH 8.5) to remove the unbound p53 protein. Then BSA solution (3%) was added to the modified surface and left for 2 h to block the free sites of Au NPs and ERGO surfaces to minimize the non-specific binding. The immunosensors were then directly subjected to immunochemical reaction with p53-Ab or to electrochemical measurements. For p53 antibody sensing, 3 μL of p53-Ab of the desired concentration in PBS, or spiked serum, were dropped onto the sensor surface and left for 1 h. Prior to electrochemical measurements, the immunosensors were washed thoroughly with 0.1% Tween-PBS (pH 7.4).

Instrumentation

The morphology of the GO and ERGO samples was examined by means of a field emission scanning electron microscope (SEM, JEOL, JSM 7401F apparatus). The chemical composition of the samples' surface was investigated by X-ray photoelectron spectroscopy, using a PHI 5600-ci spectrometer (Physical Electronics, Eden Prairie, MN). A standard aluminium X-ray source (Al Kα = 1486.6 eV) was used to record the survey spectra while a standard magnesium was used for high resolution spectra, both without charge neutralization. The C (1s) photoelectron line was used as internal standard for correcting the charging effect in the samples. Curve fitting of the XPS data was carried out with CasaXPS version 2.3.15. Micro-Raman spectroscopy was performed by using the 514 nm laser radiation of an Ar^+ laser with a circular polarization. The laser beam was focused on the sample to a spot size of 1 μm in diameter (micro-Raman spectroscopy, Renishaw Imaging Microscope WireTM).

Electrochemical measurements, including cyclic voltammetry (CV) and square wave voltammetry (SWV), were carried out using a PGSTAT 302N Autolab potentiostat/galvanostat (Eco-Chemie, The Netherlands). CV experiments were conducted at a scan rate of 100 mV s^{-1} and SWV measurements were carried out under the following conditions: the voltage was scanned from 0.8 V to −0.8 V (*vs.* Ag/AgCl reference electrode) with a step potential of 5 mV, the amplitude and the frequency were kept as 20 mV and 25 Hz, respectively. All measurements were performed in 10 mM PBS buffer pH 7.4 in the presence of a 5 mM $[Fe(CN)_6]^{3-/4-}$ redox couple at ambient temperature.

Results and discussion

Characterization of ERGO, Au NPs, and the immunosensor platform

Fig. 1 shows the SEM surface morphologies of Au NPs, ERGO, Au NP/ERGO, and p53/Au NP/ERGO. The SEM image of the Au NPs shows uniform particles (Fig. 1A), implying that colloidal Au NPs are homogeneous in terms of size and shape. The ERGO material (Fig. 1B) displays crumpled sheet-like waves with a disordered structure.[39,40]

The Au NP/ERGO image shows a number of aggregated bright dots positioned over the entire surface[41] particularly at the wrinkle sites (Fig. 1C), revealing that the Au NPs were indeed self-assembled onto the surface of thiolated ERGO. Interestingly, more dispersed and less aggregated Au NPs are seen upon the electrostatic interactions of p53 with the Au NP surface (Fig. 1D). Possibly the binding of positively charged

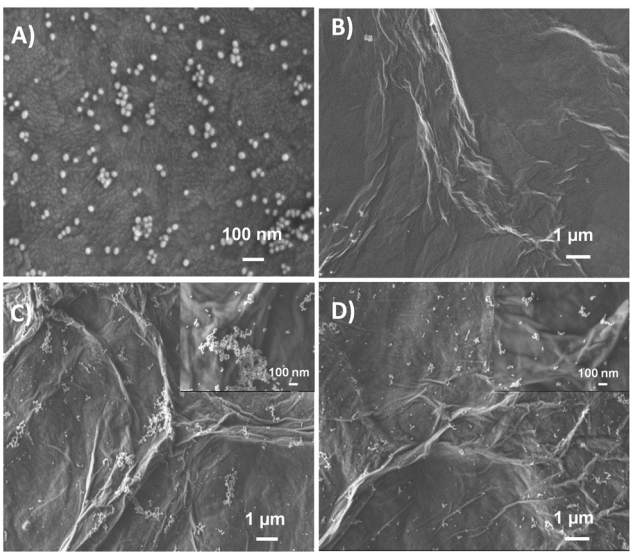

Fig. 1 SEM images of (A) Au NPs, (B) ERGO, (C) Au NP/ERGO, and (D) p53/Au NP/ERGO. Insets in (C) and (D) are high magnification images.

p53 to the negatively charged Au NPs reduced the aggregation of the NPs through steric hindrance, although the loss of some Au NPs from the ERGO surface cannot be eliminated.

The Raman spectra of the GO, ERGO and Au NP/ERGO were also recorded. Characteristic bands at 1350 and 1600 cm^{-1} due to the D and G bands[42] are observed for GO, ERGO and Au NP/ERGO surfaces (Fig. 2). There is a shift to a lower wave number in the D and G bands (to 1349 and 1598 cm^{-1}, respectively), and an increase of the I_D/I_G ratio from 0.76 to 0.81 upon the electroreduction of GO to ERGO, as expected. Interestingly, an enhancement of the Raman scattering signal for ERGO/Au NPs is observed (Fig. 2, inset, red spectrum), which originates from the surface-enhanced Raman scattering effect of Au NPs.

The immunosensor assembly was monitored by recording the XPS spectra of ERGO before and after thiolation with Cys, after Au NP modification and then upon binding of the p53 protein. Reduction of GO to ERGO was also confirmed by XPS (Fig. S3B, ESI†). The XPS survey of ERGO surfaces shows two peaks at 284.4 eV and 531 eV corresponding to the C1s and O1s, respectively, (Fig. 3A). Two additional peaks at 399 and 165 eV from the N1s and S2p are observed in the survey of Cys/ERGO, which were absent in the spectrum of ERGO. These peaks confirm the thiolation of ERGO through the amine groups of Cys and the S/N (at%) ratio was found to be 1.76.

Upon the assembly of Au NPs onto the Cys/ERGO surface (Fig. 3A), characteristic Au peaks at 84.3 and 88.0 eV are found[43] and the Au/S ratio is 3.42. Moreover, the signatures of the N1s and the S2p peaks are still observed which is a strong indication of the stability of the thiolated ERGO surface, but the lower S/N ratio (1.46) is regarded as powerful evidence of the successful Au NP/Cys/ERGO formation. After the binding

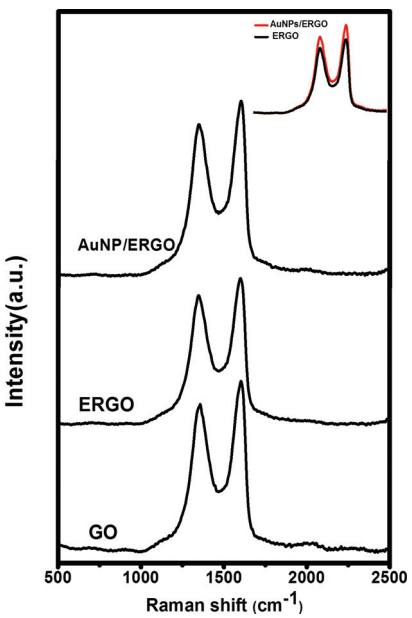

Fig. 2 The Raman spectra of the GO, ERGO and Au NP/ERGO. Inset is the overlap of the ERGO and Au NP/ERGO Raman spectra.

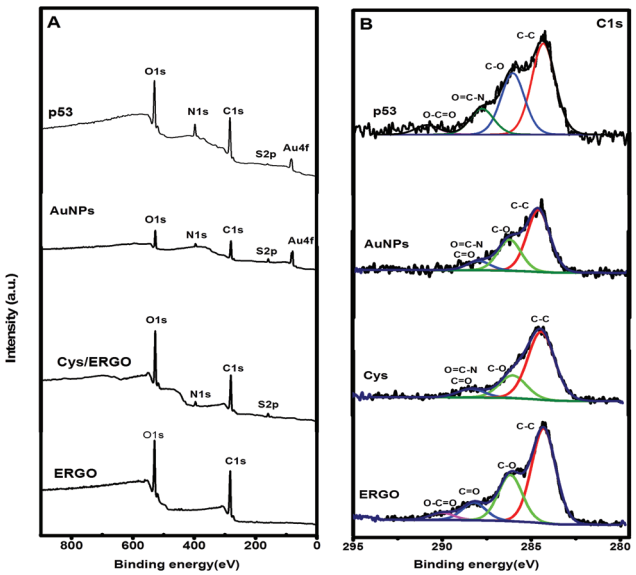

Fig. 3 X-ray photoelectron spectra for ERGO, Cys/ERGO, Au NP/ERGO and p53/Au NP/ERGO. (A) Survey and (B) C 1s core-level spectra.

of p53 onto the Au NP/ERGO surface, the Au/S ratio (0.27) is 10 times lower than before binding, and this is due to the coverage of the Au NP surface by the adsorbed bulky p53 protein.

The deconvolution of C1s spectra upon the stepwise modifications is also presented to illustrate the sensor assembly (Fig. 3B). Four components of carbon in different functional groups can be fitted for ERGO. The peaks occur at binding energies of 284.5, 286.6, 287.8 and 289.4 eV, corresponding to graphitic (C–C), epoxy (C–O), carbonyl (C═O) and carboxylic acid (O–C═O) groups, respectively. Three values at 286.6, 287.9 and 289.4 eV were obtained upon thiolation of ERGO by Cys with a shift of the C–C peak to 286.6 eV as previously reported.[44] The disappearance of the carboxylic acid (O–C═O) peak and appearance of the broad peak at 287.9 eV is indicative of the consumption of (O–C═O) groups and formation of amide bonds (O═C–N), as expected for the grafting of cysteamine onto the ERGO surface.[43,45] A similar C1s peak was obtained and deconvolution was performed for Au NP assembly onto the Cys/ERGO surface (Fig. 3B). The anchoring of p53 onto the Au NP/Cys/ERGO surface is accompanied by the reappearance of a small carboxylic acid peak.

The deconvolution of the N1s and S2p spectra of Cys/ERGO before and after Au NPs, and p53 modifications are shown in Fig. 4A. The two fitted peaks at 399.2 and 400.5 eV are assigned to C–N–C and N–C amide bonds, respectively. Moreover, S2p photoelectron spectra, consisting of a doublet peak at 164.3 and 165.5 eV, were recorded for ERGO functionalized with Cys and after the assembly of Au NPs. Upon p53 conjugation to the Au NPs' surface, a peak at ~167.5 eV was found, which may be attributed to the S bound to oxygen. The reason could be the oxygen content of p53.[46–48] The doublet peak Au4$f_{7/2}$ and Au4$f_{5/2}$ with binding energies of 84.3 and 88.0 eV, respectively,[43] (Fig. 4, curve C, bottom), confirms that

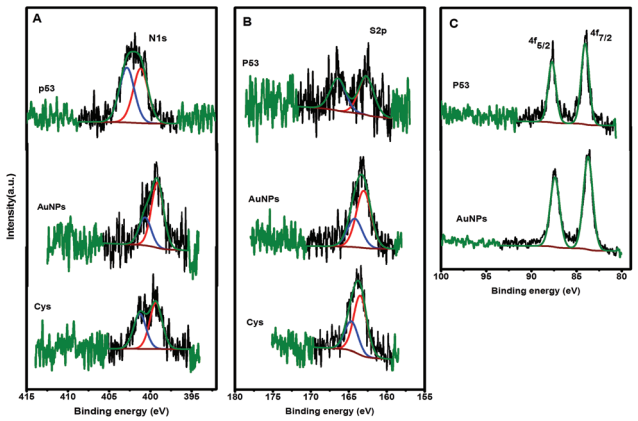

Fig. 4 High resolution of N1s, S2p and Au4f spectra for Cys/ERGO, Au NP/ERGO and p53/Au NP/ERGO.

Au NPs have been effectively assembled on the surface of thiolated ERGO sheets through the terminal SH groups. Thus, the p53/Au NP/Cys/ERGO platform was constructed as confirmed by stepwise XPS analysis.

The immunosensor fabrication steps were also monitored by recording SWVs from an equimolar solution of $[Fe(CN)_6]^{3-/4-}$ (Fig. 5). SWV voltammograms of the $[Fe(CN)_6]^{3-/4-}$ probe at the Cys/ERGO surface showed a slightly lower peak potential (from 0.056 V to 0.019 V for ERGO electrode) and a higher peak current (i_p) (Fig. 5, black and red curves). The possible reason could be the electrostatic attraction between the terminal SH and the anionic redox probes.[45] After the assembly of Au NPs onto the Cys/ERGO surface (Fig. 5, blue curve), the peak potential shifted to −0.034 V and the peak current decreased. The lower peak current might be attributed to the repulsion between the redox probe and the negatively charged Au NP/ERGO surface (the isoelecric point of Au NPs is 5.5).[49] Upon p53 protein binding onto the Au NP surface, the peak current further diminishes (Fig. 5, magenta curve) due to the steric effect of the bulky p53 protein. Finally, further decrease of the

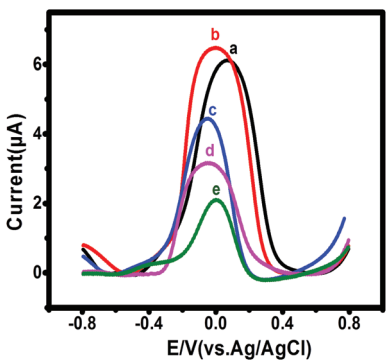

Fig. 5 SWVs of 5 mM $[Fe(CN)_6]^{3-/4-}$ probe at pH 7.4 for (a) bare ERGO, (b) Cys/ERGO, (c) Au NP/Cys/ERGO, (d) p53/Au NP/Cys/ERGO and (e) BSA/Au NP/Cys/ERGO. SWV parameters: potential range of 0.8 V to −0.8 V with a step potential of 5 mV, amplitude 20 mV and frequency 25 Hz.

i_p was observed following the BSA blocking of the p53/ERGO immunosensor surface (Fig. 5, green curve) by covering the remaining exposed Au NPs and ERGO surfaces.

Immunosensor optimization

The detection process of the p53 antibody is shown in Scheme 1. The p53 protein layer attached to the Au NP decorated ERGO was used to recognize p53 antibodies. The drop in the SWV reduction peak current (i_p) of the $[Fe(CN)_6]^{3-/4-}$ couple upon p53 Ab recognition by the immunosensor surface was used as sensor signal. An optimization study was performed prior to immunosensor application, since the immunosensor's performance might be affected by the p53 protein concentration of the p53 antibody and the time to incubate it onto the sensor's surface. The p53 concentration was varied to determine the maximum quantity of the p53 protein to be attached to the Au NP/ERGO electrode. Fig. 6A shows the response of the blocked immunosensors at different p53 protein concentrations for 1 ng mL^{-1} p53 antibody solution. The response $(i_0 - i)/i_0\%$ which represents the percentage change in the SWV peak current before and after interaction with the p53 antibody, was used for evaluation. The sensor response increased from 30 to 50 μg mL^{-1}, followed by a drop from 70 to 100 μg mL^{-1}, implying the saturation of the sensor surface at 50 μg mL^{-1}.

To confirm this finding, we performed cyclic voltammetry of the Au NP/ERGO surfaces in 0.1 M H_2SO_4 at a scan rate of 100 mV s^{-1}, before (Fig. 6B, black curve) and after p53 coupling at various concentrations from 30 to 100 μg mL^{-1} (Fig. 6B, colour curves). The cyclic voltammograms show the typical features of polycrystalline Au, with two anodic peaks at about 1.0 V related to the oxidation of the Au surface and the cathodic peak centered at ~0.57 V related to reduction of Au surface oxide.[50,51] The small shifts in peak potential are due to the instability of the pseudo Ag/AgCl reference electrode.

Upon p53 modification, the area under the Au oxidation and reduction peaks decreases as expected, with the maximum drop at 50 μg mL^{-1} p53. This confirmed the electrostatic binding of p53 on the Au NPs, and supports the optimization results of Fig. 6A, *i.e.* the coverage of Au NP surface by p53 of 50 μg mL^{-1}. By integrating the charge required for reducing the formed gold oxide in the positive sweep and by using the well accepted conversion factor 386 μC cm^{-2},[52,53] the electrochemical surface area (ECSA) of the Au NPs can be estimated. For example, the total ECSA of the Au NP coated ERGO surface before and after the binding of 50 μg mL^{-1} p53 were calculated to be 0.164 cm^2 and 0.0043 cm^2, respectively (Fig. 6B, inset). This implies that 97.4% area of Au NPs was covered by the p53 protein, and this method allows an indirect estimation of the p53 loading onto the Au NP surfaces. As shown in the inset of Fig. 6B, the coverage of the Au NPs varies with the concentration of p53 in the solution and the maximum coverage was found for 50 μg mL^{-1} p53 in good agreement with the data reported in Fig. 6A. Thus, 50 μg mL^{-1} of p53 protein were used as the optimum p53 concentration for successive experiments.

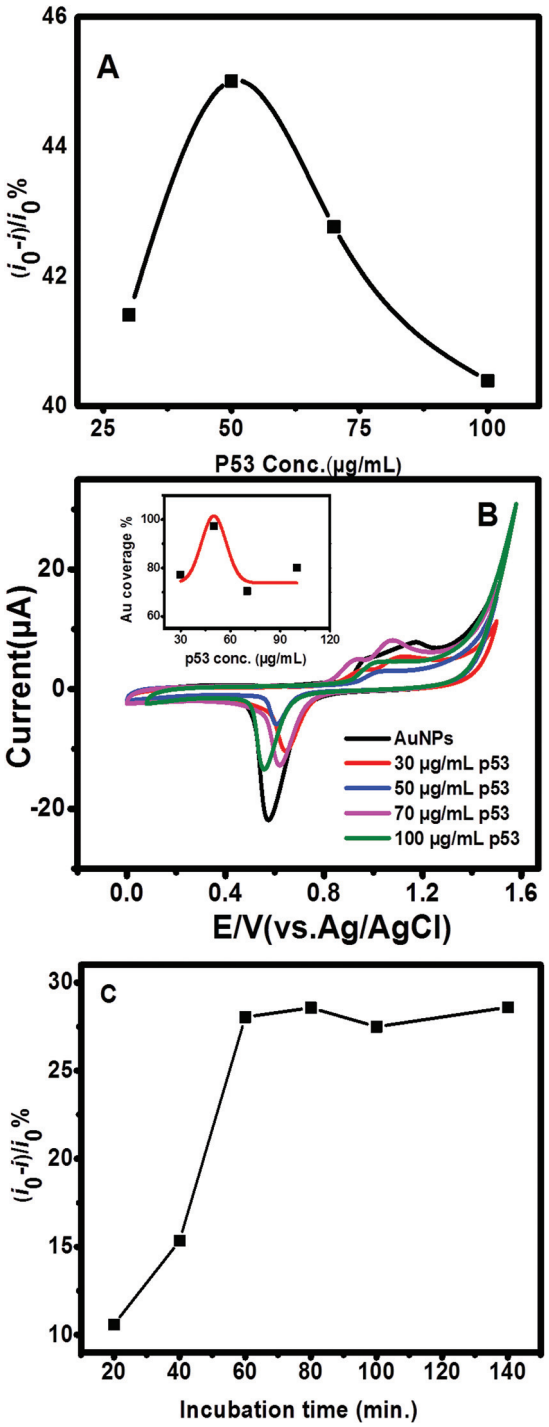

Fig. 6 (A) Effect of p53 concentration on the immunosensor response for 1 ng mL^{-1} p53 antibody in 10 mM PBS (pH 7.4) containing 5 mM $[Fe(CN)_6]^{3-/4-}$ redox couple. (B) Cyclic voltammograms of Au NP/ERGO electrodes before and after binding to p53 of concentrations 30 μg mL^{-1} to 100 μg mL^{-1} in 0.1 M H_2SO_4 at a scan rate of 100 mV s^{-1}, the inset in the panel B shows the dependence of Au NP surface coverage on the p53 concentrations. (C) Effect of p53-Ab incubation time on the immunosensor response, under the same conditions as in Fig. 5.

The incubation time to bind the p53 antibody was also optimized. The immunosensors' response at various incubation times for 1 ng mL^{-1} p53 antibody was recorded (Fig. 6C). The $(i_0 - i)/i_0$% response value increases by increasing the incubation time from 10 to 60 min, after which it levels off.

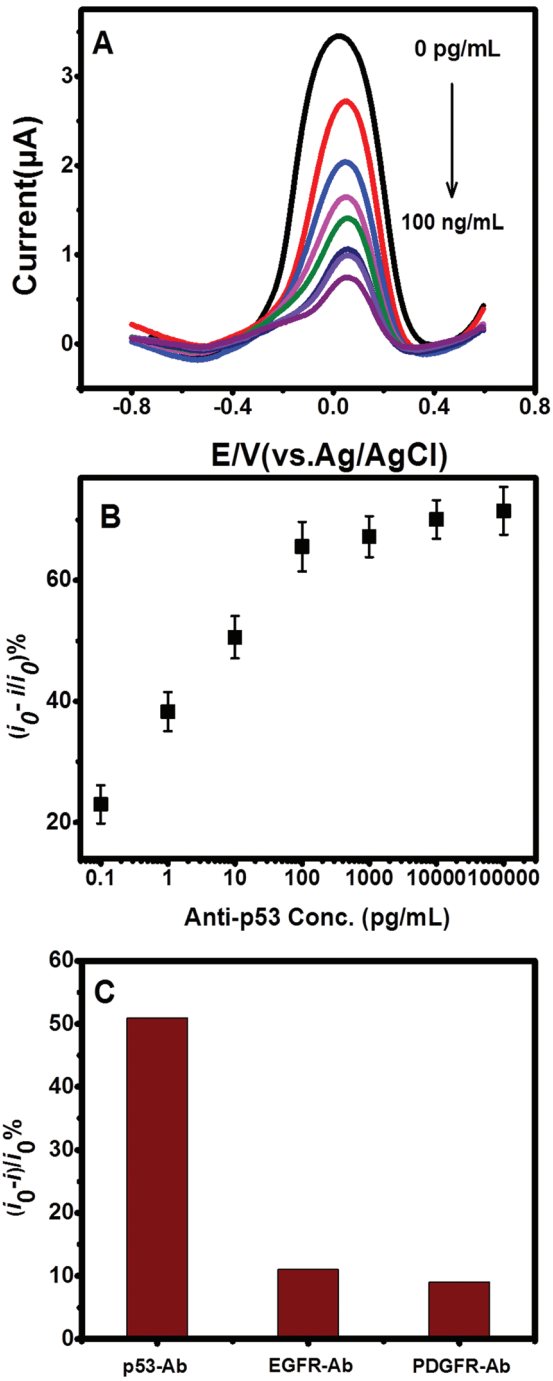

Fig. 7 (A) SWVs of the p53 immunosensing system incubated in p53 antibody solutions of concentration varying between 0.1 pg mL^{-1} to 100 ng mL^{-1}. (B) Calibration curve for detection of p53 antibodies. Error bars represent the standard deviation, n = 3. (C) The immunosensor response $(\Delta i/i_0)$% against 1 ng mL^{-1} antibodies of EGFR, PDGFRα and p53.

Thus, the optimal incubation time for further investigation was chosen to be 60 min.

p53 antibody immunosensor

For immunosensor testing, the concentration of p53 was kept at 50 μg mL^{-1} and the incubation binding time at 60 min, while the current signals were recorded for a series of p53-Ab concentrations. Fig. 7A shows that increasing concentration of the p53 antibody from 0.1 pg mL^{-1} to 100 ng mL^{-1} has led to systematically lower peak current values. The calibration plot was then constructed by plotting the $(\Delta i/i_0)\%$ *i.e.* $((i_{p53} - i_{anti\text{-}p53\ Ab})/i_{p53})\%$ against the logarithm of p53 antibody concentration (Fig. 7B). A wide dynamic range was found between 0.1 pg mL^{-1} and 100 ng mL^{-1}. The reproducibility expressed in terms of the relative standard deviation (RSD) was about 4.1% ($n = 4$) at p53 antibody concentration of 10 ng mL^{-1}. The limit of detection (LOD) of p53 Ab was determined to be 0.088 pg mL^{-1} (signal-to-noise ratio of 3). This LOD is lower than that of conventional ELISA of (0.39 ng mL^{-1}) and the microcantilever based biosensor of 20 ng mL^{-1},[21] but is higher than the one reported for the peptide based impedimetric biosensor, 0.01 pg mL^{-1},[22] probably due to the higher affinity of the selected peptide to the p53-Ab analyte.

Immunosensor selectivity and real sample testing

Control experiments were performed in the presence of some coexistent proteins as interferences to evaluate the immunosensor selectivity. Epidermal endothelial growth factor (EGFR) and platelet derived growth factor receptor alpha (PDGFRα) antibodies were utilized. The bar chart of the sensor response in terms of $(\Delta i/i_0)\%$ for these interferences is shown in Fig. 7C, which reveals that there are no significant changes in the current signal as compared to the case of the p53 antibody. These results confirm the selectivity of the immunosensor to p53 antibodies only.

We have tested the immunosensor for the detection of p53-Ab in human serum. p53 antibody concentrations were spiked into the serum, and the signal responses were recorded. The recoveries calculated from the calibration plot established in the buffer were in the range of 91.2 to 101.9% with a RSD of 1.9% to 10.3%, indicating acceptable accuracy and demonstrating that the immunosensor has the potential for detecting p53 antibodies in real samples.

Conclusions

We have successfully designed a new platform based on Au NP/ERGO for sensitive voltammetric detection of p53 antibodies in serum. ERGO films were prepared by the self-assembly method onto the surface of screen printed carbon electrodes. Au NPs were covalently bonded to thiolated ERGO films and used to bind the p53 protein. Our novel detection scheme is a label-free based assay, which avoids the need of labels and makes the antibody detection simple and rapid. The immunosensor showed a linear dynamic range and a detection limit of 0.1 pg mL^{-1} to 100 ng mL^{-1} and 0.088 pg mL^{-1}, respectively. The proposed immunosensor showed excellent analytical performance for the detection of p53 antibody with high selectivity and reproducibility. The immunosensor detected p53 antibodies from spiked serum with high recovery values. We conclude that this platform has the potential to be used in clinical applications and point-of-care diagnosis as a simple and rapid assay.

Acknowledgements

This work was made possible by support from the Natural Science and Engineering Research Council of Canada (NSERC) and Les Fonds de Recherche du Québec—Nature et Technologies (FRQNT). We acknowledge all the characterization centers including NanoQAM, Le Centre de Caractérisation Microscopique des Matériaux (CM^2). The authors thank Mr Christophe Chabanier (INRS-EMT) for helping with XPS characterization.

References

1 R. Siegel, D. Naishadham and A. Jemal, *CA-Cancer J. Clin.*, 2012, **62**, 10–29.
2 J. Joo, D. Kwon, C. Yim and S. Jeon, *ACS Nano*, 2012, **6**, 4375–4381.
3 Y. Wang, X. Zhu, M. Wu, N. Xia, J. Wang and F. Zhou, *Anal. Chem.*, 2009, **81**, 8441–8446.
4 S. Hanash, *Nature*, 2003, **422**, 226–232.
5 B. Vogelstein, D. Lane and A. J. Levine, *Nature*, 2000, **408**, 307–310.
6 D. P. Lane, *Nature*, 1992, **358**, 15–16.
7 L. J. Ko and C. Prives, *Genes Dev.*, 1996, **10**, 1054–1072.
8 A. J. Levine, *Cell*, 1997, **88**, 323–331.
9 S. Metcalfe, T. K. Wheeler, S. Picken, S. Negus and A. J. Milner, *Breast Cancer Res.*, 2000, **2**, 438–443.
10 M. M. Atta, S. A. El-Masry, M. Abdel-Hameed, H. A. Baiomy and N. E. Ramadan, *Clin. Biochem.*, 2008, **41**, 1131–1139.
11 K. S. Anderson, J. Wong, A. Vitonis, P. Crum, P. M. Sluss, J. LaBaer and D. Cramer, *Cancer Epidemiol., Biomarkers Prev.*, 2010, **19**, 859–868.
12 M. Cioffi, M. T. Vietri, P. Gazzerro, R. Magnetta, A. D'Auria, A. Durante, E. Nola, G. A. Puca and A. M. Molinari, *Lung Cancer*, 2001, **33**, 163–169.
13 J. Zhang, Z. Xu, L. Yu, M. Chen and K. Li, *PLoS One*, 2014, **9**, e99255.
14 B. Mudenda, J. A. Green, B. Green, J. R. Jenkins, L. Robertson, M. Tarunina and S. J. Leinster, *Br. J. Cancer*, 1994, **69**, 1115–1119.
15 J.-M. Portefaix, C. Fanutti, C. Granier, E. Crapez, R. Perham, J. Grenier, B. Pau and M. Del Rio, *J. Immunol. Methods*, 2002, **259**, 65–75.
16 G. Yan, D. Xing, S. Tan and Q. Chen, *J. Immunol. Methods*, 2004, **288**, 47–54.

17 S. K. Arya and S. Bhansali, *Chem. Rev.*, 2011, **111**, 6783–6809.
18 A. Rasooly and J. Jacobson, *Biosens. Bioelectron.*, 2006, **21**, 1851–1858.
19 J. F. Rusling, C. V. Kumar, J. S. Gutkind and V. Patel, *Analyst*, 2010, **135**, 2496–2511.
20 B. V. Chikkaveeraiah, A. A. Bhirde, N. Y. Morgan, H. S. Eden and X. Chen, *ACS Nano*, 2012, **6**, 6546–6561.
21 Z. W. Youzheng Zhou, Y. Wentao, T. Kai, R. Wenzhou, Q. Zhang and L. Liu, In Sensors, 2009 IEEE; IEEE: Christchurch, 2009, 819–822.
22 E. Prats-Alfonso, X. Sisquella, N. Zine, G. Gabriel, A. Guimerà, F. J. del Campo, R. Villa, A. H. Eisenberg, M. Mrksich, A. Errachid, J. Aguiló and F. Albericio, *Small*, 2012, **8**, 2106–2115.
23 S. Azzouzi, L. Rotariu, A. M. Benito, W. K. Maser, M. Ben Ali and C. Bala, *Biosens. Bioelectron.*, 2015, **69**, 280–286.
24 B. Zhang, D. Tang, B. Liu, H. Chen, Y. Cui and G. Chen, *Biosens. Bioelectron.*, 2011, **28**, 174–180.
25 X. Pang, J. Li, Y. Zhao, D. Wu, Y. Zhang, B. Du, H. Ma and Q. Wei, *ACS Appl. Mater. Interfaces*, 2015, **7**, 19260–19267.
26 S. Myung, A. Solanki, C. Kim, J. Park, K. S. Kim and K.-B. Lee, *Adv. Mater.*, 2011, **23**, 2221–2225.
27 Y. Zhang, G. M. Zeng, L. Tang, J. Chen, Y. Zhu, X. X. He and Y. He, *Anal. Chem.*, 2015, **87**, 10385–10391.
28 S. Liu, J. Yan, G. He, D. Zhong, J. Chen, L. Shi, X. Zhou and H. Jiang, *J. Electroanal. Chem.*, 2012, **672**, 40–44.
29 Q. Xi, X. Chen, D. G. Evans and W. Yang, *Langmuir*, 2012, **28**, 9885–9892.
30 A. Benvidi, A. Dehghani-Firouzabadi, M. Mazloum-Ardakani, B.-B. F. Mirjalili and R. Zare, *J. Electroanal. Chem.*, 2015, **736**, 22–29.
31 B. Cai, L. Huang, H. Zhang, Z. Sun, Z. Zhang and G.-J. Zhang, *Biosens. Bioelectron.*, 2015, **74**, 329–334.
32 Y. Fang, S. Guo, C. Zhu, Y. Zhai and E. Wang, *Langmuir*, 2010, **26**, 11277–11282.
33 M. A. Raj and S. A. John, *J. Phys. Chem. C*, 2013, **117**, 4326–4335.
34 Z. Wang, X. Zhou, J. Zhang, F. Boey and H. Zhang, *J. Phys. Chem. C*, 2009, **113**, 1871–1878.
35 A.-M. J. Haque, H. Park, D. Sung, S. Jon, S.-Y. Choi and K. Kim, *Anal. Chem.*, 2012, **84**, 1871–1878.
36 W. S. Hummers and R. E. Offeman, *J. Am. Chem. Soc.*, 1958, **80**, 1339–1339.
37 A.-E. Radi, X. Muñoz-Berbel, M. Cortina-Puig and J.-L. Marty, *Electroanalysis*, 2009, **21**, 1624–1629.
38 A. Ambrosi, M. T. Castañeda, A. J. Killard, M. R. Smyth, S. Alegret and A. Merkoçi, *Anal. Chem.*, 2007, **79**, 5232–5240.
39 D. Lin, J. Wu, M. Wang, F. Yan and H. Ju, *Anal. Chem.*, 2012, **84**, 3662–3668.
40 Q. Wei, K. Mao, D. Wu, Y. Dai, J. Yang, B. Du, M. Yang and H. Li, *Sens. Actuators, B*, 2010, **149**, 314–318.
41 J. Chen, H. Lin, X. Li, X. Zhao, F. Hao and S. Dong, *Electrochim. Acta*, 2011, **56**, 6026–6032.
42 K. N. Kudin, B. Ozbas, H. C. Schniepp, R. K. Prud'homme, I. A. Aksay and R. Car, *Nano Lett.*, 2008, **8**, 36–41.
43 W. Cheng, S. Dong and E. Wang, *Langmuir*, 2003, **19**, 9434–9439.
44 J. A. Smith, M. Josowicz and J. Janata, *J. Electrochem. Soc.*, 2003, **150**, E384–E388.
45 A. Mars, C. Parolo, N. Raouafi, K. Boujlel and A. Merkoci, *J. Mater. Chem. B*, 2013, **1**, 2951–2955.
46 R. M. Ferrizz, R. J. Gorte and J. M. Vohs, *Catal. Lett.*, 2002, **82**, 123–129.
47 J. Wang, R. Ma, Z. Zhou, G. Liu and Q. Liu, *Sci. Rep.*, 2015, **5**, 1–9.
48 D. Briggs, *Surf. Interface Anal.*, 1981, **3**, v.
49 I. Arnaud, J.-P. Abid, C. Roussel and H. H. Girault, *Chem. Commun.*, 2005, **6**, 787–788.
50 D. Dickertmann, J. W. Schultze and K. J. Vetter, *J. Electroanal. Chem. Interfacial Electrochem.*, 1974, **55**, 429–443.
51 F. J. Rodríguez Nieto, G. Andreasen, M. E. Martins, F. Castez, R. C. Salvarezza and A. J. Arvia, *J. Phys. Chem. B*, 2003, **107**, 11452–11466.
52 *Electroanalytical Chemistry: A Series of Advances*, ed. R. Woods and A. J. Bard, Marcel Dekker, New York, 1980, vol. 9.
53 R. Szamocki, A. Velichko, C. Holzapfel, F. Mücklich, S. Ravaine, P. Garrigue, N. Sojic, R. Hempelmann and A. Kuhn, *Anal. Chem.*, 2007, **79**, 533–539.